Available online at www.sciencedirect.com
SCIENCE DIRECT®
International Journal of Heat and Mass Transfer 49 (2006) 850–867
International Journal of HEAT and MASS TRANSFER
www.elsevier.com/locate/ijhmt

Modeling of low-density lipoprotein (LDL) transport in the artery—effects of hypertension

Ning Yang, Kambiz Vafai *

Department of Mechanical Engineering, University of California, Bourns Hall, Riverside, CA 92521-0425, United States

Received 12 June 2005; received in revised form 13 September 2005
Available online 23 November 2005

Abstract

A robust four-layer model is presented to describe the LDL transport in the arterial wall coupled with the transport in the lumen. The endothelium, intima, internal elastic lamina (IEL) and media are all treated as macroscopically homogeneous porous media and the volume-averaged porous media equations are employed to model various layers, with Staverman filtration and osmotic reflection coefficients introduced to account for selective permeability of each porous layer to certain solutes. The physiological parameters within the various layers are obtained from literature. The set of governing equations for fluid flow and mass transport is descretized using a finite element scheme based on the Galerkin method of weighted residuals. Filtration velocity and LDL concentration profiles are developed at different locations for various clinical conditions. The results are consistent with previous numerical and experimental studies. Effects of hypertension and boundary conditions are discussed based upon the present model. Furthermore, the effects of pulsatile flows on LDL transport in the arterial wall are studied in some detail. Compared to previous transport models, the newly developed model is found to be a more robust tool for investigation of LDL accumulation within different arterial wall layers for various clinical conditions. This will be helpful in understanding the role of transmural transport processes in the initiation and development of atherosclerosis.

1. Introduction

Atherosclerosis is a disease usually located within large arteries. It is well accepted that the early atherogenesis tends to be hallmarked by an abnormally high accumulation of macromolecules, i.e. LDL, within the arterial wall. This fact suggests that the macromolecular transport in the arterial wall must have some impact on the initiation and development of atherosclerosis. However, it is still unknown whether atherogenesis is initiated by this abnormally high accumulation in the intima, or whether this abnormality is only a secondary effect due to atherogenesis [1]. As a result, mathematical modeling of the macromolecular transport, for example, LDL, in the arterial wall has received considerable attention in recent years. Prosi et al. [2] have classified these models in three major categories. The simplest models used so far are *wall-free* models, in which the arterial wall is substituted by a simplified boundary condition. Rappitsch and Pertold [3] and Wada and Karino [4] applied these models for the analysis of the macromolecular transport in the arterial wall. A more realistic approach is named *lumen-wall* models, which couple the transport within the lumen and the wall. In these models, the arterial wall is simplified as a homogeneous monolayer. Such models, originally proposed by Moore and Ethier [5], have been used to study the mass transport of LDL within the arterial wall by Stangeby and Ethier [6,7]. The most realistic models are *multilayer models*, which break the arterial wall down into several layers and model the transport within the wall, either at the microscopic [8–11] or macroscopic [2,12–14] levels.

* Corresponding author. Tel./fax: +1 951 827 2135.
E-mail address: vafai@engr.ucr.edu (K. Vafai).

0017-9310/$ - see front matter © 2005 Elsevier Ltd. All rights reserved.
doi:10.1016/j.ijheatmasstransfer.2005.09.019

Nomenclature

C	dimensionless LDL concentration, c/C_0
C_0	reference inflow LDL concentration [nmol/mm^3]
c	dimensional LDL concentration [nmol/mm^3]
$\bar{c}$	average LDL concentration
D	diffusivity [mm^2/s]
D'	diffusivity per unit length [mm/s]
K	permeability [mm^2]
K'	permeability per unit length [mm]
k	effective volumetric first-order reaction rate coefficient [1/s]
L	longitudinal length of the artery [mm]
L_p	hydraulic conductivity [mm]
l	fiber length per unit volume [mm/mm^3]
N''_s	absolute molar flux of solutes [nmol/(mm^2 s)]
n	normal direction
P_d	diffusive permeability [mm/s]
p	hydraulic pressure
R	radius of the arterial lumen [mm]
R_u	universal gas constant
r	dimensional radial coordinates [mm]
r_f	radius of a fiber [nm]
r_{sol}	radius of a solute [nm]
T	absolute temperature [K]
T_{cl}	period [s]
t	dimensional time [s]
U_0	reference bulk inflow velocity [mm/s]
U_{cl}	centerline velocity at the lumen inlet [mm/s]
u	dimensional axial velocity [mm/s]
V	velocity vector [mm/s]
v	dimensional radial velocity [mm/s]
x	dimensional axial coordinates [mm]

Greek symbols

δ	parameter used to account for the fluctuation of pulsatile flows
ε	porosity
μ	dynamic viscosity [g/(mm s)]
μ'	effective dynamic viscosity of a medium [g/(mm s)]
π	osmotic pressure
ρ	density [g/mm^3]
σ_d	Staverman osmotic reflection coefficient
σ_f	Staverman filtration reflection coefficient
ϕ_f	partition coefficient

Superscript

f	fluid

Subscript

e	effective property

Other symbol

$\langle\rangle$	"local volume average" of a quantity

To the best of our knowledge, the Staverman–Kedem–Katchalsky membrane equations [15] are usually used to model the transport processes in the endothelium and internal elastic lamina (IEL) in the previous *multilayer* models. However, the traditional Staverman–Kedem–Katchalsky equations have at least couple of substantial disadvantages: it is derived based on the existence of steady state condition, which is in conflict with the real physiological conditions existing within both endothelium and IEL; it ignores the boundary effects on the flow across the membrane, which is not valid when the boundaries of the porous membrane have to be accounted for.

The main focus of the present study is to develop a new fundamental four-layer model for the description of the mass transport in the arterial wall coupled with the mass transport in the arterial lumen. The endothelium, intima, IEL and media layers are all treated as macroscopically homogeneous porous media and mathematically modeled using proper types of the volume averaged porous media equations, with the Staverman filtration and osmotic reflection coefficients employed to account for selective permeability of each porous layer to certain solutes. In particular, the effects of hypertension on the LDL transport within the arterial wall are studied based on our new mathematical model, to identify possible factors that might be responsible for enhanced arterial wall uptake of LDL under hypertensive conditions. Moreover, five different categories of boundary conditions, partially taken from the aforementioned models, are presented to examine the differences in fluid flow and mass transport characteristics in the arterial wall due to different types of boundary conditions. Finally, the effects of pulsation on the LDL transport within the arterial wall are discussed in some detail.

2. Analysis

2.1. Anatomy

The typical anatomical structure of an arterial wall is shown schematically in Fig. 1. Going from the lumen to the most external layer, a large artery is comprised of the following five layers: glycocalyx, endothelium, intima, media, and adventitia. The luminal glycocalyx is a thin layer of macromolecules which is believed to cover the plasma membrane of a single layer of endothelial cells, and the entrance of the intercellular junctions. The thickness of the glycocalyx is usually less than 100 nm (average thickness 60 nm) [16,17]. Immediately in contact with the

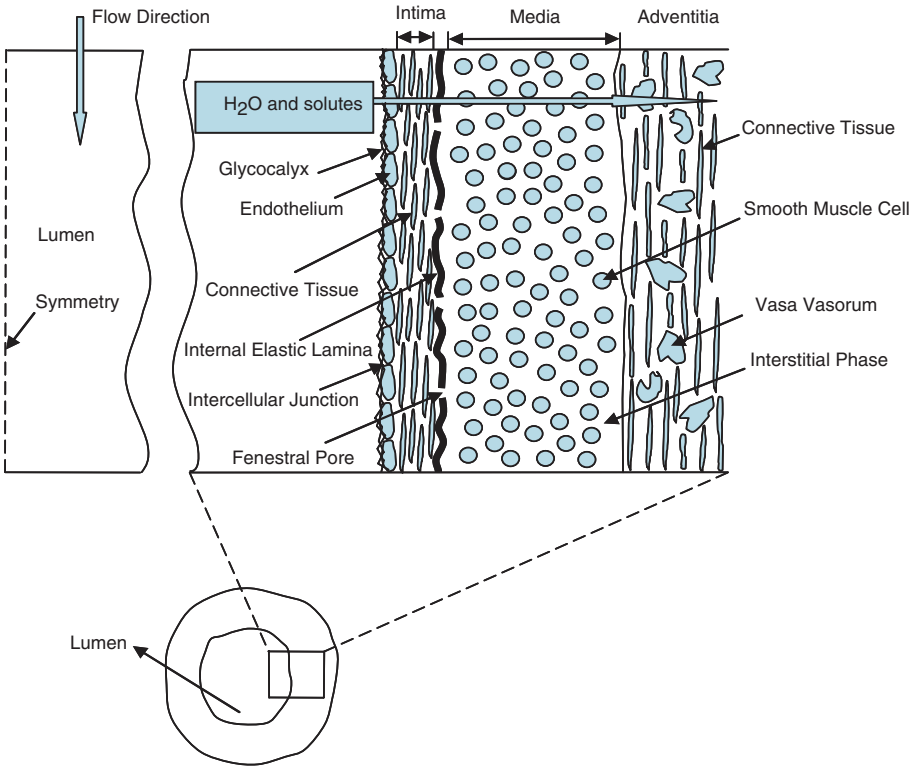

Fig. 1. Transverse section of a large artery.

glycocalyx is endothelium, a single layer of endothelial cells, which are elongated in the direction of blood flow. Endothelial cells are interconnected through intercellular junctions. Internal elastic lamina (IEL), an impermeable elastic tissue with fenestral pores, is lying between intima and media. In contrast to the media, which contains alternating layers of smooth muscle cells and elastic connective tissue, the intima is mainly comprised of proteoglycan and collagen fibers. The media layer is surrounded by loose connective tissue, the adventitia, in which there are some capillaries (lymphatic and vasa vasorum). Except via transport from luminal blood supplies, proteins can be transported from the adventitia to the media through the vasa vasorum.

2.2. Mathematical formulation

A new four-layer mathematical model is developed for the description of LDL transport in the arterial wall, coupled with the mass transport in the arterial lumen. The effects of the luminal glycocalyx are neglected in the present study due to its negligible effect. Fig. 2 shows the schematic diagram of the idealized artery geometry under consideration.

2.2.1. Lumen

The blood is considered to be an incompressible Newtonian fluid. The blood flow in the arterial lumen is described by the Navier–Stokes and continuity equations

$$\rho\frac{\partial V}{\partial t}+\rho V\cdot\nabla V=-\nabla p+\mu\nabla^2 V \tag{1}$$

$$\nabla\cdot V=0 \tag{2}$$

where V is the velocity vector, p is the pressure, and ρ and μ are the density and dynamic viscosity of blood.

The concentration field in the arterial lumen is computed via the mass transport equation

$$\frac{\partial c}{\partial t}+V.\nabla c=D\nabla^2 c \tag{3}$$

where c is the LDL concentration and D is the LDL diffusivity within the blood.

2.2.2. Endothelium and internal elastic lamina

The endothelium and internal elastic lamina (IEL) are treated as biological porous membranes. The Staverman filtration and osmotic reflection coefficients are employed to account for selective rejection of species by the membranes and for the effects of osmotic pressure. The volume averaged governing equations are [18–21]

$$\nabla\cdot\langle V\rangle=0 \tag{4}$$

$$\frac{\rho}{\varepsilon}\frac{\partial\langle V\rangle}{\partial t}+\frac{\mu}{K}\langle V\rangle=-\nabla\langle p\rangle^{\mathrm{f}}+R_{\mathrm{u}}T\sigma_{\mathrm{d}}\nabla\langle c\rangle+\mu'\nabla^2\langle V\rangle \tag{5}$$

$$\frac{\partial\langle c\rangle}{\partial t}+(1-\sigma_{\mathrm{f}})\langle V\rangle.\nabla\langle c\rangle=D_{\mathrm{e}}\nabla^2\langle c\rangle \tag{6}$$

where ε is the porosity, K the permeability, μ' the effective dynamic viscosity of the medium, which will be taken as $\frac{\mu}{\varepsilon}$

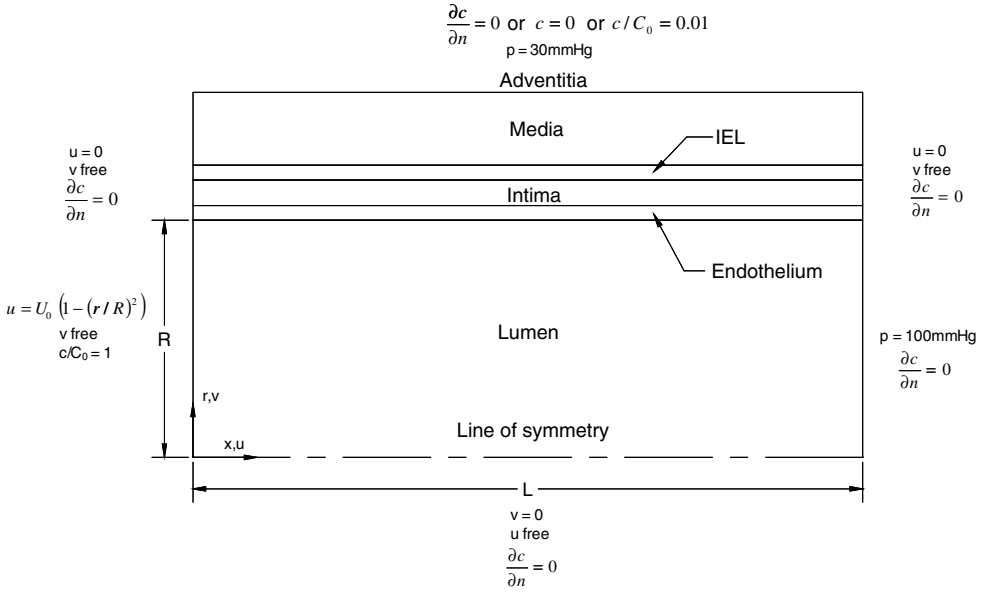

Fig. 2. Schematic illustration of the geometric artery.

[18,20] and D_e is the effective LDL diffusivity in the medium. The parameters σ_f and σ_d are the Staverman filtration and osmotic reflection coefficients (to account for selective permeability of biological membranes to certain solutes), respectively, for LDL, T is the absolute temperature of the medium, and R_u is the universal gas constant. The symbol "$\langle\rangle$" denotes the local volume average of a quantity [18]. The superscript 'f' refers to the local volume average inside the fluid [18,22].

2.2.3. Intima and media

The intima and media are modeled as macroscopically homogeneous porous media. Since the porous media are selectively permeable to certain species such as LDL, the Staverman filtration reflection coefficient has to be introduced to account for this effect. The osmotic effect in the transport modeling is not included in this part since the maximum osmotic pressure gradient in the medial layer is far below the hydraulic pressure gradient [10]. Therefore, the volume averaged governing equations of the intima and media layers are [18–21]

$$\nabla\cdot\langle V\rangle=0 \tag{7}$$

$$\frac{\rho}{\varepsilon}\frac{\partial\langle V\rangle}{\partial t}+\frac{\mu}{K}\langle V\rangle=-\nabla\langle p\rangle^{f}+\mu'\nabla^2\langle V\rangle \tag{8}$$

$$\frac{\partial\langle c\rangle}{\partial t}+(1-\sigma_f)\langle V\rangle.\nabla\langle c\rangle=D_e\nabla^2\langle c\rangle+k\langle c\rangle \tag{9}$$

where k is the effective volumetric first-order reaction rate coefficient. Fry [12] and Huang and Tarbell [10] have cited that the uptake of solutes by the smooth muscle cells in the media can be approximated as an irreversible first-order reaction. The symbol "$\langle\rangle$" indicating averaged values will be dropped from the V, p, and c from here on for brevity.

2.3. Computational geometry and boundary conditions

The artery is idealized as a straight axi-symmetric geometry with a luminal radius of $R=3.1$ mm and a longitudinal length of $L=124$ mm [7,14]. The thickness of each wall layer is shown in Table 1. Eqs. (1)–(9) can be solved if suitable boundary conditions are provided.

2.3.1. Steady flows

The boundary conditions for the steady flow are shown in Fig. 2: a fully developed (parabolic) velocity profile ($u=U_0(1-(r/R)^2)$) at the inlet of the arterial lumen is taken and it is assumed that $u=0$, both at the inlet and outlet sections of the arterial wall. In addition we employ the zero cross flow condition which exists on the axis of symmetry ($v=0$), and constant pressure at the outlet of the arterial lumen and the media adventitia interface. Effects of other fundamental types of boundary conditions are explored later in this study. At the interfaces between the lumen, endothelium, intima, IEL and media continuity of velocity and shear stress is applied.

The concentration boundary conditions are: $c/C_0=1$ at the lumen inlet, zero normal diffusive mass flux at the axis of symmetry, at the lumen outlet, and the inlet and outlet of the arterial wall. Three types of boundary conditions are emplored at the media adventitia interface: $c/C_0=0$, $c/C_0=0.01$, and $\frac{\partial c}{\partial n}=0$ [2]. Note that C_0 is the reference

Table 1
Thickness of each wall layer of the artery [2,14,23]

Wall layer	Thickness (μm)
Endothelium	2.0
Intima	10.0
IEL	2.0
Media	200.0

concentration at the lumen inlet for LDL. These boundary conditions are reflective of the physiological conditions that exist within an artery [6,7,14].

The concentration boundary conditions at the interface between the lumen, endothelium, intima, IEL, and media are

$$\left[(1-\sigma_f)vc - D_e\frac{\partial c}{\partial n}\right]\Big|_+ = \left[(1-\sigma_f)vc - D_e\frac{\partial c}{\partial n}\right]\Big|_- \tag{10}$$

where v is the velocity in radial direction. Note that in the arterial lumen the reflection coefficient σ_f is zero and the effective diffusivity D_e is the LDL diffusivity within the blood flow.

2.3.2. Pulsatile flows

The major difference between the boundary conditions for steady flows and pulsatile flows mainly lies in the velocity profile applied at the lumen inlet. In the present study, the inlet velocity profile is assumed to be axi-symmetric, which is specified as [24]

$$u(t) = U_{cl}(t)\left(1-(r/R)^2\right) \tag{11}$$

where U_{cl} is the centerline velocity at the lumen inlet defined by a simple time-dependent sinusoidal function to characterize pulsatile flows in the artery as [25]

$$U_{cl}(t) = U_0(1+\delta\sin(2\pi t/T_{cl})) \tag{12}$$

where T_{cl} is the period of the pulsatile blood flow and the parameter δ is used to account for the fluctuation of the pulsatile blood flow during each cardiac cycle. All the other boundary conditions are kept the same as those shown in Fig. 2 except that the species concentration boundary condition applied at the media adventitia interface is $\partial C/\partial n = 0$. The initial conditions for both blood flow and species concentration are taken directly from the solutions for steady flows.

2.4. Physiological parameters

The physiological properties for various wall layers used in our model are calculated based upon appropriate pore theory [26], fiber matrix models [8–10,26–29] and in vivo and in vitro experiments.

2.4.1. Endothelium and internal elastic lamina

Traditionally, transport characterization across the endothelium and IEL is represented by the Staverman–Kedem–Katchalsky membrane transport equations given as

$$V = \frac{K'}{\mu}(\Delta p - \sigma_d\Delta\pi) \tag{13}$$

$$N_s'' = D_e'\Delta c + (1-\sigma_f)V\bar{c} \tag{14}$$

where V is the velocity vector of bulk flow across the membrane, N_s'' the absolute molar flux of the solute across the membrane, Δp the pressure differential across the membrane, $\Delta\pi$ the corresponding osmotic pressure differential, Δc the solute concentration differential, K' the permeability per unit length, D_e' the effective diffusivity per unit length, $\bar{c}$ the mean solute concentration over the membrane, and σ_f and σ_d are the Staverman filtration and osmotic reflection (which account for the selective permeability of biological membranes to certain solutes) coefficients respectively. Note that $\frac{K'}{\mu}$ and D_e' are the so called hydraulic conductivity and diffusive permeability of the membrane, traditionally denoted as L_p and P_d, respectively.

An aspect that requires attention in modeling the endothelium and IEL layers is the absence (to the best of authors' knowledge) of any experimental data in the literature for the permeability K and diffusivity D_e for either the endothelial or IEL layers. However, if we make the reasonable approximation that the transport is one-dimensional within these layers and neglect the boundary effects, we can convert the hydraulic conductivity and the diffusive permeability to the permeability K and diffusivity D_e as follows:

$$K = \mu L_p\Delta x \tag{15}$$

$$D_e = D_e'\Delta x \tag{16}$$

where Δx is the thickness of the biological membrane.

Applying the pore theory with the appropriate size of the molecules and of the pores, some investigators [2,14] have derived $L_{p,\text{endothelium}} = 3\times10^{-9}$ mm^2 s/g, $L_{p,\text{IEL}} = 3.05\times10^{-7}$ mm^2 s/g, $D'_{e,\text{endothelium}} = 3\times10^{-10}$ mm/s, and $D'_{\text{IEL}} = 1.59\times10^{-6}$ mm/s for LDL. It should be noted that Prosi et al. [2] have also cited that $D'_{e,\text{endothelium}} = 3\times10^{-10}$ mm/s is too low when compared with the available clinical data. Studies by Tarbell [17] have suggested that the value of the endothelial diffusive permeability for LDL is similar for the aorta of humans, monkeys, rabbits, and pigeons, falling down in the range of 1.1×10^{-8}–2.6×10^{-7} mm/s. Given the absence of experimental data for the endothelial permeability in large arteries, we choose $D'_{e,\text{endothelium}}$ to be of the order of 10^{-8} mm/s in this study based on the clinical data of Tarbell [17].

The corresponding permeability K and diffusivity D_e are calculated from Eqs. (15) and (16). The values of the filtration reflection coefficients are taken from Prosi et al. [2]. The osmotic reflection coefficients is treated the same as the filtration reflection coefficients for simplicity and lack of reliable specific data.

2.4.2. Intima and media

There is also a lack of any pertinent experimental data for the permeability K and diffusivity D for the intima. Huang et al. [9], using a heterogeneous fiber matrix theory, which consists of proteoglycan and collagen components, have predicted that the hydraulic permeability K and diffusivity D of the subendothelial intima are two orders of magnitude larger than the corresponding values measured in the media.

Table 2
Physiological parameters used in the numerical simulation

Layers	Parameters	Value	Ref. no.
Lumen	Density ρ, g/mm^3	1.057×10^{-3}	
	Diffusivity D, mm^2/s	2.87×10^{-5}	[14]
	Dynamic viscosity μ, g/(mm s)	3.70×10^{-3}	[14]
Endothelium	Permeability K, mm^2	4.32×10^{-15}	[2,14]
	Effective diffusivity D_e, mm^2/s	6.00×10^{-11}	[2,14,17]
	Dynamic viscosity μ, g/(mm s)	0.72×10^{-3}	[2]
	Filtration reflection coefficient σ_f	0.9979	[2]
	Osmotic reflection coefficient σ_d	0.9979	[2]
	Porosity ε	0.0005	[32]
Intima	Permeability K, mm^2	2.00×10^{-10}	[9]
	Effective diffusivity D_e, mm^2/s	5.40×10^{-6}	[9]
	Dynamic viscosity μ, g/(mm s)	0.72×10^{-3}	[2]
	Filtration reflection coefficient σ_f	0.8272	[2]
	Porosity ε	0.983	[9]
IEL	Permeability K, mm^2	4.392×10^{-13}	[2,14]
	Effective diffusivity D_e, mm^2/s	3.18×10^{-9}	[2,14]
	Dynamic viscosity μ, g/(mm s)	0.72×10^{-3}	[2]
	Filtration reflection coefficient σ_f	0.9827	[2]
	Osmotic reflection coefficient σ_d	0.9827	[2]
	Porosity ε	0.002	[33]
Media	Permeability K, mm^2	2.00×10^{-12}	[9,34]
	Effective diffusivity D_e, mm^2/s	5.00×10^{-8}	[9,35]
	Dynamic viscosity μ, g/(mm s)	0.72×10^{-3}	[2]
	Filtration reflection coefficient σ_f	0.8836	[2]
	Reaction rate coefficient k, 1/s	3.197×10^{-4}	[2]
	Porosity ε	0.258	[10,14]

Curry [26] has demonstrated that the Staverman reflection coefficients σ_f and σ_d for the convective transport in the fiber matrix can be expressed as

$$\sigma_f = \sigma_d = (1-\phi_f)^2 \tag{17}$$

where ϕ_f is the partition coefficient, defined based on the distribution of spaces available to a certain spherical molecule in a random fiber matrix [27] made of infinitely long, stiff rods satisfying the Poisson distribution. This leads to

$$\phi_f = \exp\left(-(1-\varepsilon)\left(2\frac{r_{sol}}{r_f}+\frac{r_{sol}^2}{r_f^2}\right)\right) \tag{18}$$

where ε is the porosity defined as

$$\varepsilon = 1-\pi r_f^2 l \tag{19}$$

and r_f, r_{sol} are the radii of fiber and solute respectively, and l is the total length of the combined fibers per unit volume.

Typically LDL radius is about 11 nm [30,31], and the porosities for the intima and media are 0.983 and 0.258, respectively [9,10,14]. The fibers in the intima and media have radii of 2.31 nm [9] and 3.22 nm [10] respectively. The resulting filtration reflection coefficients for the intima and media are 0.3 and 1 correspondingly, which indicates that the LDL transport in the media is dominated by diffusion. This result is perplexing since it has been well accepted that convective effects dominate the LDL transport in the artery wall [7]. Due to this discrepancy and the absence of experimental data for the reflection coefficients of the intima and media, Prosi et al.[2]'s data are used in the present investigation. The complete specification of values of key parameters required for numerical simulation is provided in Table 2.

3. Computational approach

The finite element method (FEM) is employed for the numerical simulations. The set of governing equations (Eqs. (1)–(9)) is first nondimensionalized and discretized into the algebraic equations using Galerkin-based FEM. The detailed procedure of this application is well documented in [36]. Two-dimensional, four-noded square elements are used in the present simulation. The resulting algebraic equations are solved using the Newton–Raphson solution algorithm. This approach has a rate of convergence superior to those of both successive substitution and segregated algorithm. The major drawback of using this method, is that it is prohibitively expensive for three-dimensional problems. A fine mesh is implemented near the fluid–porous and porous–porous interfaces to capture the steep gradients in species concentration due to the expected large rejection fluxes at the interfaces. Extensive numerical experimentation is also performed to attain grid-independent results for all the field variables. The time-step independence of the numerical results is verified for pulsatile flows. A relative convergence criterion of 10^{-6} is applied for all the field

variables. Aspects related to simulation of biological processes and detection of pathogens are utilized in this work [37–39].

4. Results and discussion

In the present work, the transport of LDL within the arterial wall, coupled with the mass transport through the arterial lumen, is investigated for various physiologically pertinent conditions. Typical values for the physiological parameters are utilized. The reference bulk inflow velocity U_0 is chosen as 338 mm/s [14], while the reference inflow concentration for LDL at the inlet C_0 is taken as 28.6×10^{-3} nmol/mm^3 [40,41]. The transmural pressure under normal physiological conditions is taken as 70 mmHg, which is slightly less than physiological pressure [23]. It should be noted that steady state conditions are assumed to have been reached except in the last section, where the effects of pulsation will be studied in some detail.

4.1. Validation of the physiological parameters

The benchmarking of the physiological parameters used in this study is performed against the experimental data of Meyer et al. [23] and numerical results of Prosi et al. [2] reported in Table 3. The comparison is made for the different interfaces encountered along the radial direction. These are the lumen endothelium interface, intima IEL interface, IEL media interface, central part of the media ($r = 3.214$ mm), and media adventitia interface. It should be noted that our numerical results are displayed at the midsection longitudinally of the arterial wall.

The filtration velocity computed from our model is 2.31×10^{-5} mm/s, which is almost 30% off from the results given by Meyer et al. [23] and Prosi et al. [2]. Their filtration velocities were 1.78×10^{-5} mm/s and 1.76×10^{-5} mm/s, respectively. This deviation can be acceptable since the calculated filtration velocity is well within the range of experimental values measure by Tedgui and Lever [42] at the same transmural pressure.

Table 3
Comparison between the values of the filtration velocity and species concentration taken from literature [2,23] and the present model

		Meyer	Prosi ($C = 0$)	Present model ($C = 0$)	Prosi ($C = 10^{-2}$)	Present model ($C = 10^{-2}$)	Prosi ($\partial C/\partial n = 0$)	Present model ($\partial C/\partial n = 0$)
Filtration velocity (mm/s)		1.78×10^{-5}	1.76×10^{-5}	2.31×10^{-5}	1.76×10^{-5}	2.31×10^{-5}	1.76×10^{-5}	2.31×10^{-5}
Species concentration	Lumen endothelium interface	1.026	1.0262	1.0246	1.0262	1.0246	1.0262	1.0246
	Intima IEL interface	N/A	2.716×10^{-2}	3.983×10^{-2}	2.727×10^{-2}	3.983×10^{-2}	2.717×10^{-2}	3.983×10^{-2}
	IEL media interface	1.00×10^{-2}	8.58×10^{-3}	1.033×10^{-2}	8.62×10^{-3}	1.033×10^{-2}	8.59×10^{-3}	1.033×10^{-2}
	Media ($r = 3.214$ mm)	2.50×10^{-3}	2.23×10^{-3}	2.687×10^{-5}	2.73×10^{-3}	2.689×10^{-5}	2.271×10^{-3}	2.687×10^{-5}
	Media adventitia interface	1.00×10^{-2}	0.00	0.00	1.00×10^{-2}	1.00×10^{-2}	8.518×10^{-4}	1.152×10^{-7}

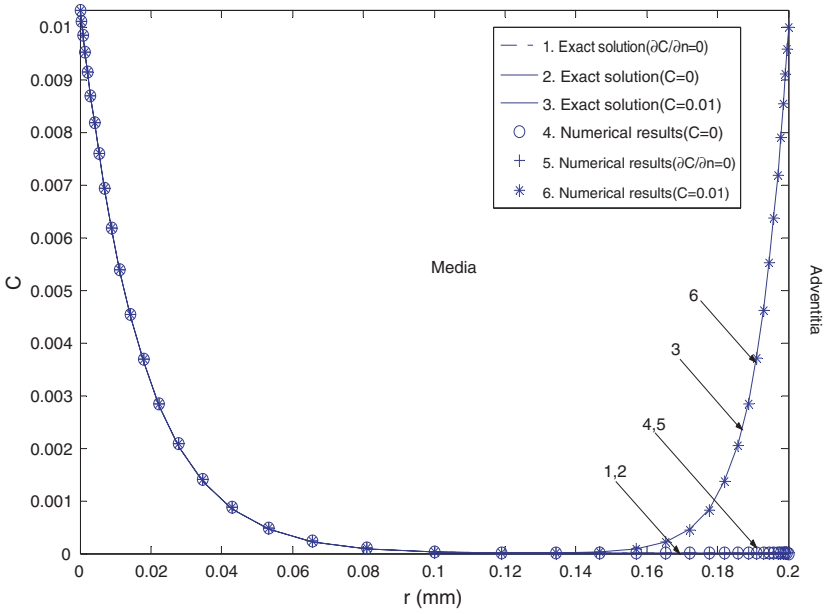

Fig. 3. Comparison between the numerical dimensionless LDL profiles in the media for three different types of concentration boundary conditions at the media adventitia interface and the exact solutions.

The numerical species concentrations at each interface are quite close to experimental data by Meyer et al. [23] and numerical results by Prosi et al. [2] except in the media layer. There is a relatively large difference between our results and the results from Meyer et al. [23] and Prosi et al. [2] in the media layer. To verify the present numerical code, a comparison between the numerical result for species profiles in the media and an exact solution is done. This comparison is displayed in Fig. 3. The exact solution is derived based on an assumption that the LDL transport in the media is one-dimensional, with constant filtration velocity. It can be seen from Fig. 3 that the present numerical results are in excellent agreement with the exact solutions. It should be noted that Truskey [43] and Morris et al. [44] have reported that the chemical reaction coefficient for LDL is 1.4×10^{-4} 1/s. This value is also used in the numerical simulation. It turns out that the reaction coefficient by Truskey [43] and Morris et al. [44], like that given by Prosi et al. [2], is also too high when compared with the experimental data by Meyer et al. [23]. Due to a lack of satisfactory experimental or theoretical prediction for the LDL reaction coefficient in the media, we will keep relying on the parameter values given in Table 2.

4.2. Species distribution across the arterial wall under normal physiological condition

Fig. 4 shows the computed species profiles for LDL at the midsection longitudinally of the arterial wall with a transmural pressure of 70 mmHg. The influence of three different types of species boundary condition ($c/C_0=0$, $c/C_0=0.01$, and $\frac{\partial c}{\partial n}=0$) at the media adventitia interface is compared. Note that the nonhomogeneous Dirichlet boundary condition ($c/C_0=0.01$) [2] is used to account for the transport of LDL from the adventitia to the media through the vasa vasorum. It can be clearly seen in Fig. 4 that the effect of different types of the outer boundary condition on the intima and IEL layers is negligible. It has also been demonstrated that there is no difference in the species distribution through all the layers, regardless of whether the homogeneous Dirichlet boundary condition ($c/C_0=0$) or Neumann boundary condition ($\frac{\partial c}{\partial n}=0$) is utilized. This might be due to an extremely low LDL concentration in the media due to high reaction coefficient, which makes the species concentration independent of the boundary conditions [14]. Moreover, Fig. 4 illustrates that there is a slight increase in LDL concentration along the radial direction within the intima. This is perhaps due to the presence of the IEL, which acts as a major barrier to large macromolecules [13,23]. The present work confirms that the intact endothelium offers the major resistance to the LDL transport through the arterial wall.

4.3. Effects of hypertension

The effects of hypertension on the LDL transport in the arterial wall are studied based on the present model, in an

Table 4
Input parameters used for testing effects of hypertension

Case number	Transumral pressure (mmHg)	Endothelial diffusivity (mm^2/s)	Ref. no.
1	70	6.00×10^{-11}	[2,14,17]
2	120	6.00×10^{-11}	[2,14,17]
3	160	6.00×10^{-11}	[2,14,17]
4	160	2.40×10^{-10}	[6]

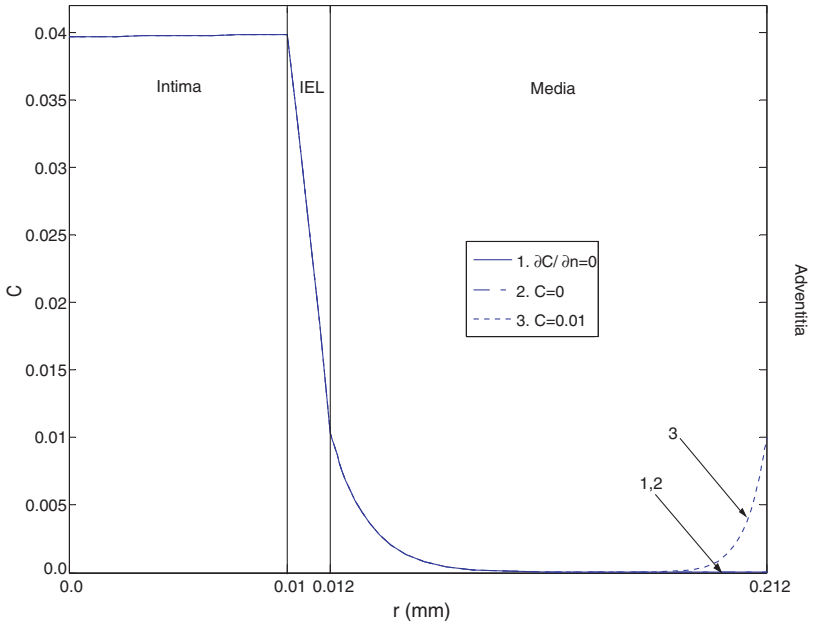

Fig. 4. Effects of the different concentration boundary conditions at the media adventitia interface on the computed dimensionless LDL concentration profiles at the midsection longitudinally of the arterial wall.

attempt to explain how the hypertension increases the uptake of LDL by the arterial wall. Four different cases are studied and the input parameters are displayed in Table 4. Case 1 represents the normal physiological condition, with a transmural pressure of 70 mmHg and a normal endothelial LDL diffusivity of 6.0×10^{-11} mm^2/s. The effects of transmural pressure are tested in cases 2 and 3, simply by increasing pressure to 120 mmHg and 160 mmHg, respectively. Case 4 accounts for the effects of both increased endothelial LDL diffusivity and transmural pressure. The pressure-linked increase of endothelial LDL diffusivity might be explained by the so called "stretching effects" [23], namely straining of the endothelial layer associated with changes in pressure. Stangeby and Ethier [6] have cited that the estimated endothelial LDL diffusive permeability at 160 mmHg is four times greater

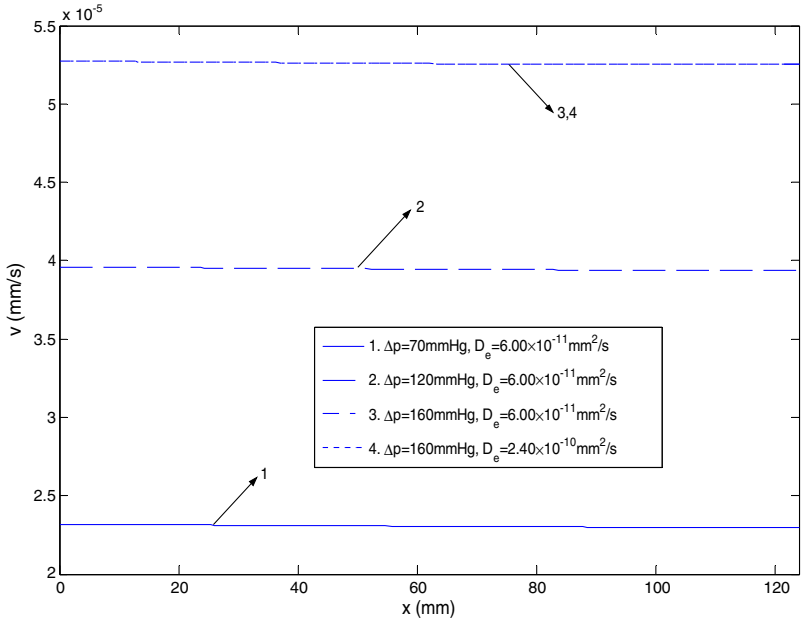

Fig. 5. Computed filtration velocity profiles along the lumen endothelium interface based upon the different values of the lumen outlet pressure.

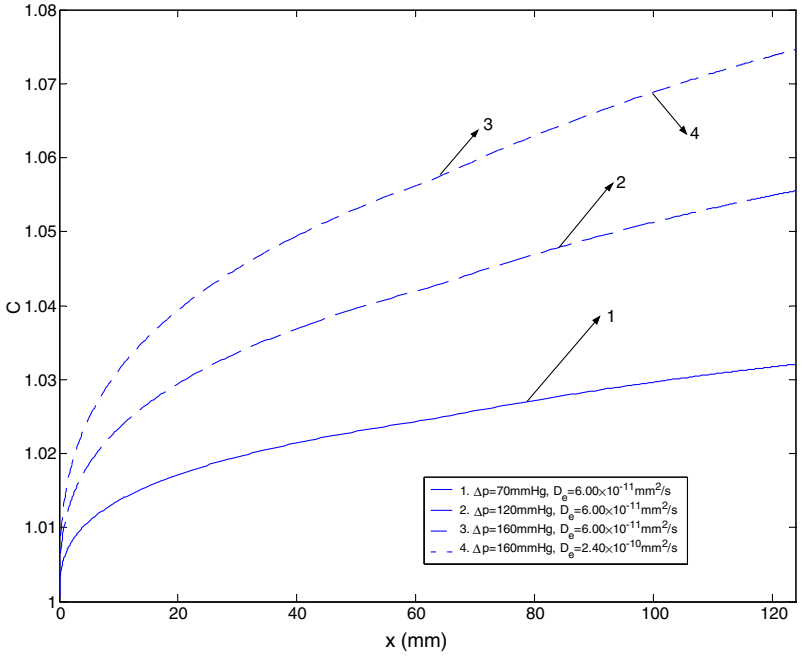

Fig. 6. Computed dimensionless LDL concentration profiles along the lumen endothelium interface for the steady flow model based upon the different values of the lumen outlet pressure.

than the value measured at normal vascular pressure. Therefore, an increased endothelial LDL diffusivity of 2.4×10^{-10} mm^2/s at a transmural pressure of 160 mmHg is used in the present study. Note that the species concentration boundary condition applied at the media adventitia interface is $\frac{\partial c}{\partial n} = 0$.

The influence of transmural pressure on the filtration velocity profile at the lumen endothelium interface is illustrated in Fig. 5. The average magnitudes of the numerical filtration velocity are 2.31×10^{-5} mm/s, 3.95×10^{-5} mm/s, and 5.26×10^{-5} mm/s at the transmural pressure of 70 mmHg, 100 mmHg, and 120 mmHg, respectively. These results are within the range of experimental measurement by Tedgui and Lever [42] and close to the numerical results by Stangeby and Ethier [6]. It should be noted that the filtration velocity drops slightly along the lumen endothelium interface. This is due to a decrease in the transmural pressure along the longitudinal direction. It is also noted that an increase in the endothelial diffusivity has a weak effect on the filtration velocity. This means

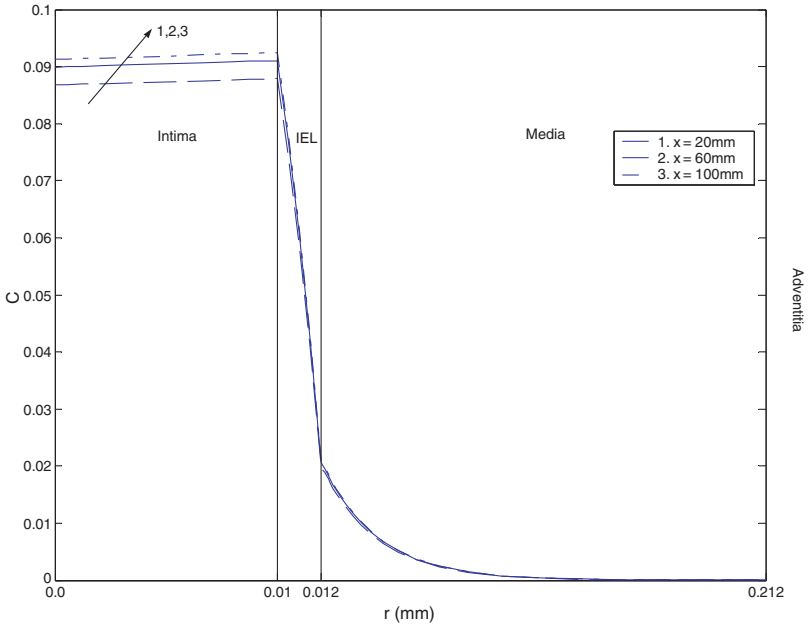

Fig. 7. Computed dimensionless LDL concentration profiles across the different layers at different axial positions $x = 20$ mm, 60 mm, and 100 mm for case 4 of Table 4.

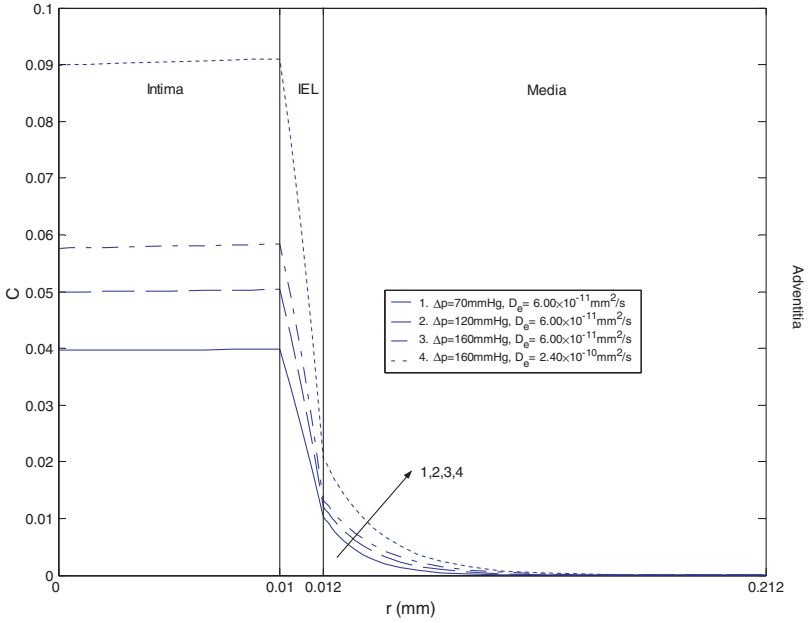

Fig. 8. Computed dimensionless LDL concentration profiles across the different layers for the steady flow model based upon the different values of the lumen outlet pressure. The numerical results are taken at the midsection of the arterial wall.

the influence of osmotic pressure on the endothelium and IEL can be negligible when compared to hydraulic pressure.

Fig. 6 illustrates the effects of transmural pressure on the LDL "concentration polarization", i.e. the accumulation of LDL at the lumen endothelium interface due to the higher resistance offered by the endothelium [45–47]. As it can be seen, transmural pressure has a significant impact on the species accumulation at the lumen endothelium interface. As the transmural pressure increases, the species accumulation is found to increase substantially. This might be explained by an increase in the convective rejection fluxes as the transmural pressure increases. As the endothelial diffusivity increases, the LDL concentration at the interface drops very slightly.

The impact of the "concentration polarization" on the LDL transport across the endothelium is examined in Fig. 7. It can be seen that the uptake of LDL into the intima is slightly dependent of axial location, while this dependence diminishes significantly in the IEL and media layers. This interesting result suggests the elevated species accumulation at the lumen endothelium interface leads to a higher species concentration in the intima layer. However, this higher species accumulation produces only minor effects on the species profiles in the IEL and media layers. It should be noted that this conclusion is in conflict with the numerical results of Stangeby and Ethier [6]. This is mainly because Stangeby and Ethier [6] lump the intima, IEL and media together and therefore neglect the impact of IEL as a major resistance for macromolecules.

Fig. 8 illustrates the influence of transmural pressure and endothelial diffusivity on the species concentration within the different layers. It is evident that the LDL uptake within different layers is largely affected by the transmural pressure and endothelial diffusivity. More specifically, increasing the transmural pressure to 160 mmHg while maintaining the normal value of endothelial LDL diffusivity (case 3) results in an almost 50% increase in the average species concentration as compared to the normal condition (case 1). On the other hand, when there is four-folder increase in the endothelial LDL diffusivity at 160 mmHg (case 4), the mean LDL concentration in the wall increases by a factor of 2.3 as compared to case 1. This result is close to the experimental measurements by Deng et al. [48] and Warty et al. [49]. Our results suggest that a pressure-induced increase in the endothelial diffusivity, combined with pressure-driven convection, most probably is a major determinant of the LDL transport across the arterial wall, which might explain increased atherosclerosis susceptibility in the presence of hypertension. In contrast, concentration polarization only plays a minor role in the enhanced LDL uptake within the arterial wall at higher transmural pressure. This contention is consistent with the conclusions by Meyer et al. [23] and Stangeby and Ethier [6] except that the present study demonstrates pressure-driven convection also plays an essential role in hypertension.

Table 5
Different boundary condition categories

Boundary interface	Model #1		Model #2		Model #3		Model #4		Model #5	
	Velocity	Species	Velocity	Species	Velocity	Species	Velocity	Species	Velocity	Species
Arterial wall inlet	$u=0$ v free	$\partial C/\partial n=0$	$u=0$ $v=$ const	$C=1$	$u=0$ $v=$ const	$C=0.01$	$u=0$ v free	$\partial C/\partial n=0$	$u=0$ $v=$ const	$\partial C/\partial n=0$
Arterial wall outlet	$u=0$ v free	$\partial C/\partial n=0$	traction free	$\partial C/\partial n=0$	traction free	$\partial C/\partial n=0$	traction free	$\partial C/\partial n=0$	$u=0$ v free	$\partial C/\partial n=0$
Lumen outlet	$p=100$ mmHg	$\partial C/\partial n=0$	traction free	$\partial C/\partial n=0$	traction free	$\partial C/\partial n=0$	traction free	$\partial C/\partial n=0$	$p=100$ mmHg	$\partial C/\partial n=0$
Media adventitia interface	$p=30$ mmHg	$\partial C/\partial n=0$	$p=-70$ mmHg	$\partial C/\partial n=0$	$p=-70$ mmHg	$\partial C/\partial n=0$	$p=-70$ mmHg	$\partial C/\partial n=0$	$p=30$ mmHg	$\partial C/\partial n=0$
Ref. no.	Present study		[7]		[6]		[14]		Present study	

4.4. Effects of boundary conditions

It is important to examine differences in fluid flow and mass transport characteristics due to different types of boundary conditions. A comprehensive synthesis of literature revealed five primary categories for boundary conditions of fluid flow and mass transport within the arterial wall. These are listed in Table 5. The major differences between these models are at the arterial wall inlet, arterial wall outlet, lumen outlet, and media adventitia interface. The boundary conditions applied at all the other interfaces are the same as those shown in Fig. 2. Note that the species concentration boundary condition applied at the media adventitia interface for all these models is $\frac{\partial c}{\partial n} = 0$.

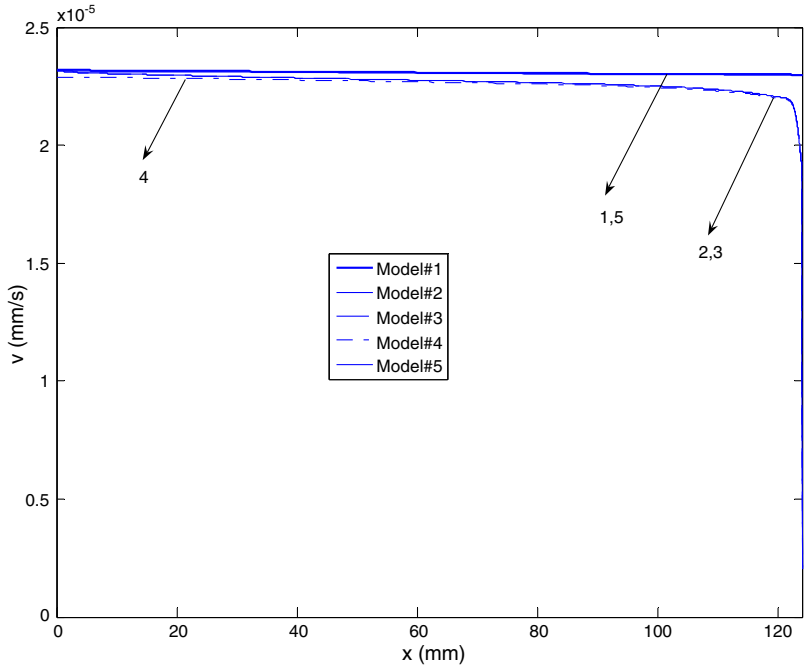

Fig. 9. Comparison of filtration velocity profiles at the lumen endothelium interface based on different types of boundary conditions listed in Table 5.

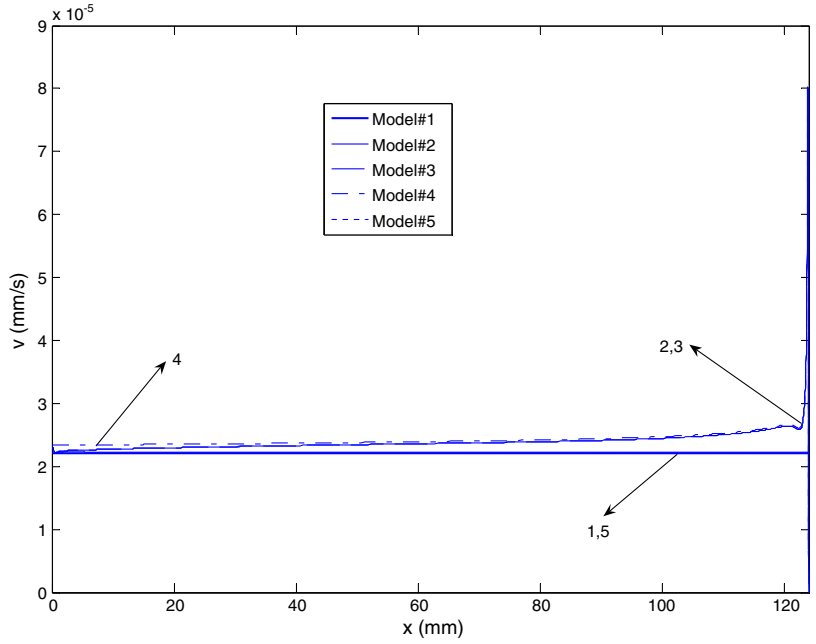

Fig. 10. Comparison of filtration velocity profiles at the central part of the media ($r = 3.214$ mm) based on different types of boundary conditions listed in Table 5.

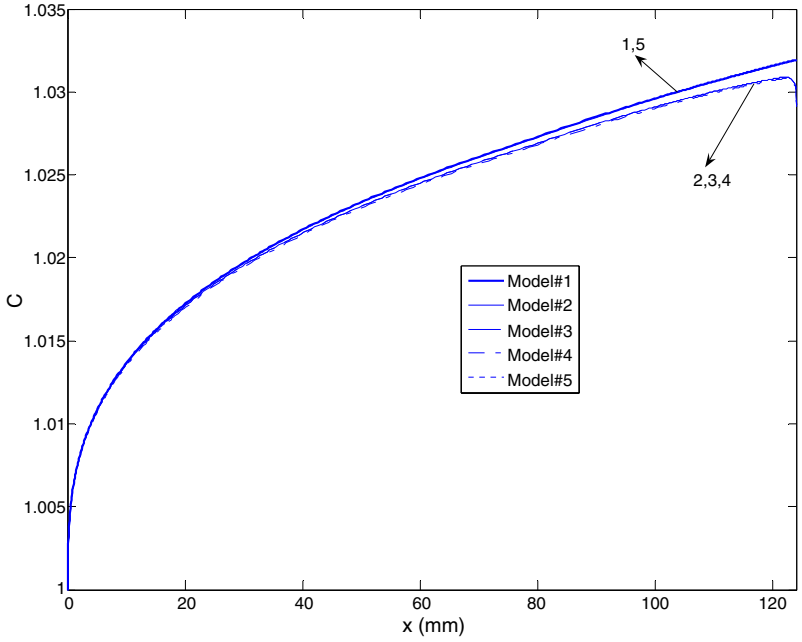

Fig. 11. Comparison of dimensionless LDL concentration profiles at the lumen endothelium interface based on different types of boundary conditions listed in Table 5.

The influence of different types of boundary conditions on the filtration velocity profiles across the arterial wall is presented in Figs. 9 and 10, by illustrating the velocity profiles at the lumen endothelium interface and central part of the media ($r = 3.214$ mm) respectively. As can be seen the velocity profiles for models 1 and 5 are almost the same while models 2–4 produce almost the same results. Compared to models 1 and 5, models 2–4 produce a significant jump in the filtration velocity around the outlet.

Fig. 11 illustrates the effects of different types of boundary conditions on the LDL "concentration polarization" at the lumen endothelium interface. It is clear that different types of boundary conditions play a minor role in the LDL accumulation at the interface. Similar to the

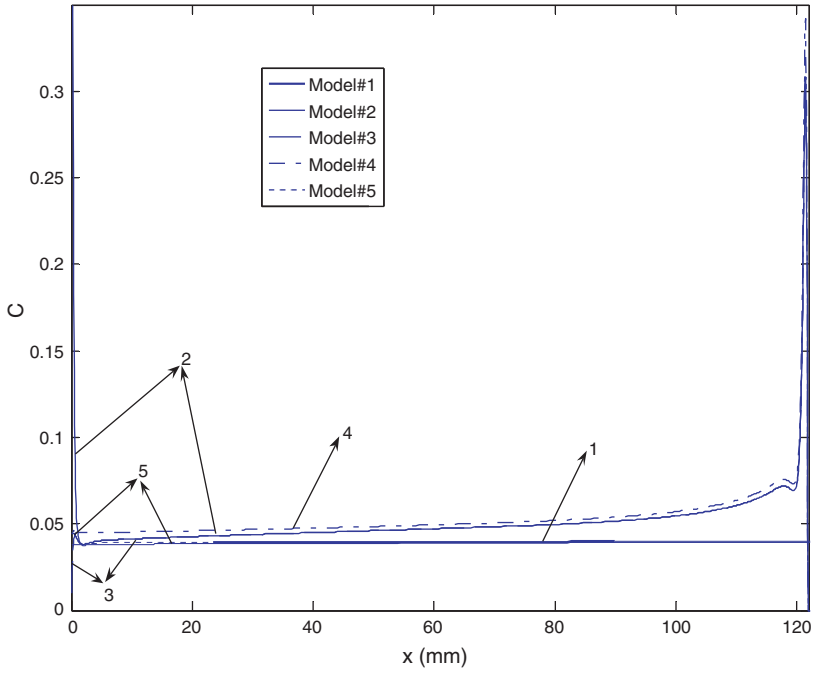

Fig. 12. Comparison of dimensionless LDL concentration profiles at the endothelium intima interface based on different types of boundary conditions listed in Table 5.

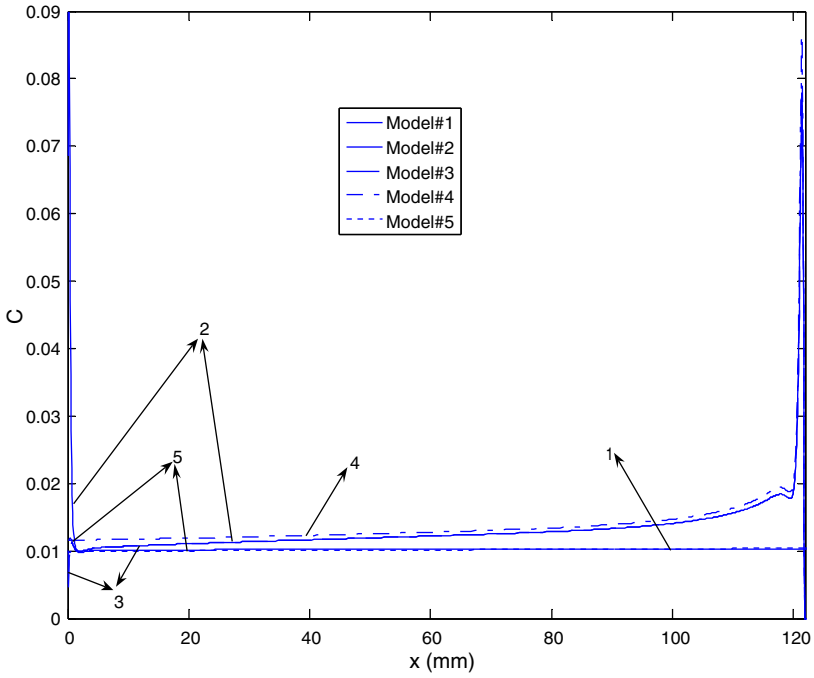

Fig. 13. Comparison of dimensionless LDL concentration profiles at the IEL media interface based on different types of boundary conditions listed in Table 5.

filtration velocity profiles, the species profiles for models 2–4 are almost the same while those for models 1 and 5 are close to each other. It is worth noting with respect to Fig. 11 for the lumen endothelium interface that a slight deviation in the LDL concentration exists between models 1 and 5 and models 2–4, which is caused by the big jump in the filtration velocity around the outlet for models 2–4.

The impact of different types of boundary conditions on the LDL distribution within the arterial wall is presented in Figs. 12 and 13, by demonstrating the species profiles at the endothelium intima and IEL media interfaces respectively. It is evident that the LDL concentration profiles within the arterial wall are substantially dependent of different types of boundary conditions. More specifically, the species profiles for models 1 and 5 almost collapse each other. The

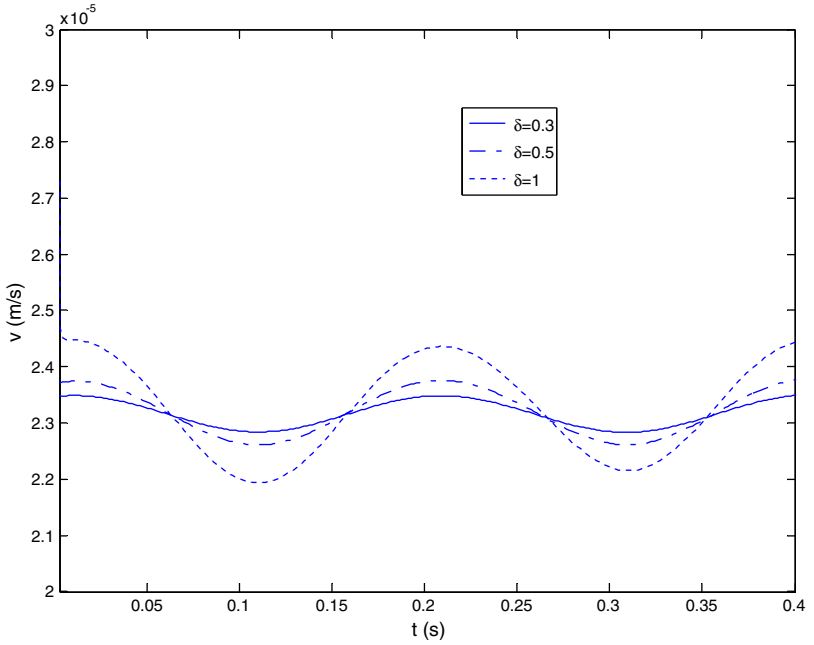

Fig. 14. Effects of pulsatile flows on the filtration velocity at the lumen endothelium interface.

same can be found for models 2 and 3. It can be clearly seen that models 2, 3 and 5 produce a jump in the species concentration at the wall inlet while models 2–4 yield a jump in the species concentration at the wall outlet. Generally, model 1 forms the lower bound while model 4 forms the upper bound.

In general, the results in the present work indicate that different types of boundary conditions have a significant impact on the velocity and LDL concentration profiles within the arterial wall. The traction-free boundary condition yields a substantial jump in the filtration velocity around the outlet. The boundary conditions employed at the wall inlet and outlet has a far more pronounced effect on the LDL distribution within the arterial wall than the velocity profile. Moreover, the LDL "concentration polarization" at the lumen endothelium interface is found to be

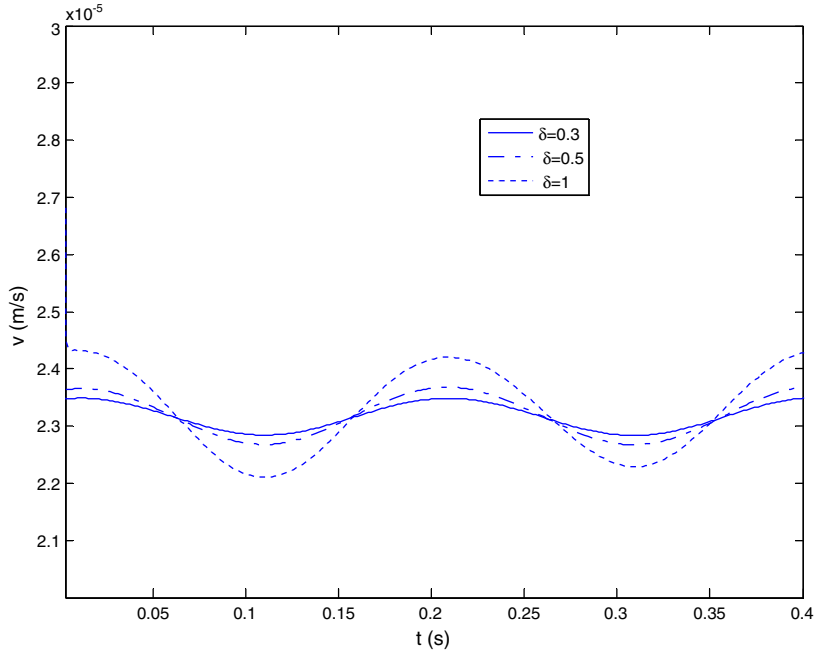

Fig. 15. Effects of pulsatile flows on the filtration velocity at the intima IEL interface.

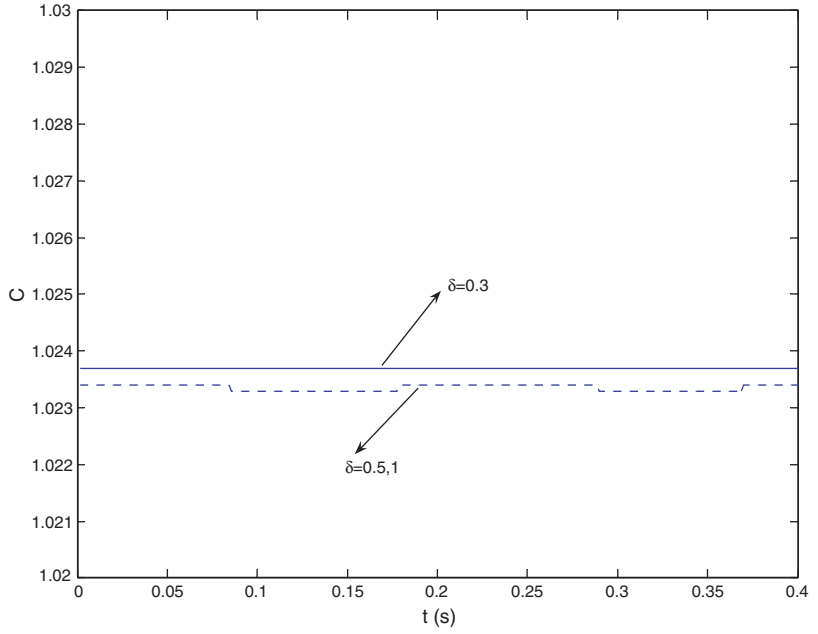

Fig. 16. Effects of pulsatile flows on the LDL accumulation at the lumen endothelium interface.

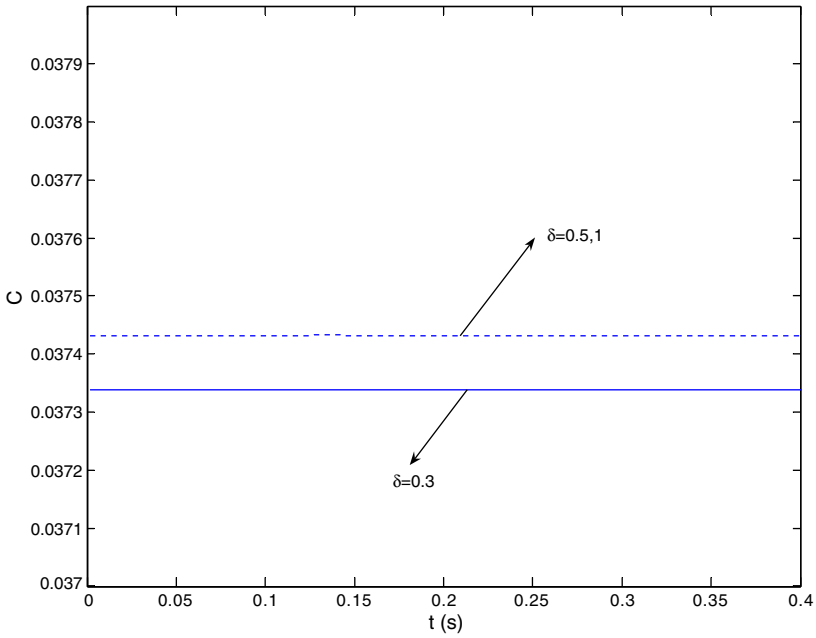

Fig. 17. Effects of pulsatile flows on the LDL concentration at the intima IEL interface.

almost independent of different types of boundary conditions.

4.5. Effects of pulsatile flows

It is now well accepted that sites where atherosclerosis develops is usually at places where the vessels have sudden changes in geometry. One of the major characteristics at these sites is that wall shear stresses are low or change rapidly in time or space [50–54]. As such the effects of pulsatile flows on the mass transport in these regions should not be ignored. Hence it is essential to study the effects of pulsatile flows on the LDL transport within the arterial wall. Here we take the period of the pulsatile flow as $T_{cl} = 0.2$ s [25]. The parameter δ is set to be 0.3, 0.5, or 1. It should be noted that the numerical results are all taken at the midsection (longitudinally) of the arterial wall.

Figs. 14 and 15 illustrate the effects of pulsatile flows on the filtration velocity at the lumen endothelium interface and intima IEL interface respectively. As expected as the parameter δ increases, the magnitude of fluctuation of the filtration velocity increases. It is noticed that the magnitude of fluctuation of the filtration velocity is relatively small when compared to the time-averaged filtration velocity for each cycle. This suggests that the effects of pulsatile flows on the filtration velocity across the arterial tissue are damped out.

Figs. 16 and 17 demonstrate the effects of pulsatile flows on the LDL concentration at the lumen endothelium interface and intima IEL interface respectively. It is clear that the impact of pulsation on the LDL transport across the arterial tissue is negligible for a simple straight axi-symmetric geometry. This is due to the large resistance offered by the arterial tissue.

5. Conclusions

The transport of LDL in the arterial wall, coupled with the transport in the lumen has been investigated based on a newly developed four-layer model. The endothelium, intima, IEL and media are all treated as macroscopically homogeneous porous media and modeled using the volume-averaged porous media equations. The numerical results are found to be in good agreement with those from the previous experimental and numerical studies under various clinical conditions.

The effects of hypertension and boundary conditions are examined in some detail based on the comprehensive model presented in this work. The results of the present investigation demonstrate that a pressure-induced increase of endothelial diffusive permeability, plus pressure-driven convective flow, is mainly responsible for the enhanced LDL uptake at higher transmural pressure, which might explain increased atherosclerosis susceptibility in the presence of hypertension. It is found that the filtration velocity and LDL concentration profiles in the arterial wall are significantly dependent of different types of boundary conditions. The traction-free boundary condition leads to a significant jump in the filtration velocity profile near the outlet. The species concentration profile within the arterial wall is found to be quite sensitive to the boundary conditions employed at the inlet and outlet.

Moreover, effects of pulsation are discussed in the present study. The pulsatile flows play a minor role in the LDL transport within the arterial wall when a straight axi-symmetric geometry is considered.

Generally, the presented four-layer model is shown to be a more robust tool to model the macromolecular transport in the arterial wall coupled with the transport in the lumen

when compared to the previous transport models. However, a number of additional efforts are required to determine the physiological parameters for each arterial wall layer more accurately. Furthermore, an important aspect which needs further investigation is with respect to pulsation and transient effects on LDL transport at places where the artery is curved, bifurcated, or has sudden change in flow geometry.

References

[1] C.R. Ethier, Computational modeling of mass transfer and links to atherosclerosis, Ann. Biomed. Eng. 30 (2002) 461–471.

[2] M. Prosi, P. Zunino, K. Perktold, A. Quarteroni, Mathematical and numerical models for transfer of low-density lipoproteins through the arterial walls: a new methodology for the model set up with applications to the study of disturbed luminal flow, J. Biomech. 38 (2005) 903–917.

[3] G. Rappitsch, K. Perktold, Pulsatile albumin transport in large arteries: a numerical simulation study, J. Biomech. Eng. 118 (1996) 511–519.

[4] S. Wada, T. Karino, Computational study on LDL transfer from flowing blood to arterial walls, in: T. Yamaguchi (Ed.), Clinical Applications of Computational Mechanics to the Cardiovascular System, Springer, Berlin, 2000, pp. 157–173.

[5] J.A. Moore, C.R. Ethier, Oxygen mass transfer calculations in large arteries, J. Biomech. Eng. 119 (1997) 469–475.

[6] D.K. Stangeby, C.R. Ethier, Coupled computational analysis of arterial LDL transport—effects of hypertension, Comput. Meth. Biomech. Biomed. Eng. 5 (2002) 233–241.

[7] D.K. Stangeby, C.R. Ethier, Computational analysis of coupled blood-wall arterial LDL transport, J. Biomech. Eng. 124 (2002) 1–8.

[8] F. Yuan, S. Chien, S. Weinbaum, A new view of convective–diffusive transport processes in the arterial intima, J. Biomech. Eng. 133 (1991) 314–329.

[9] Y. Huang, D. Rumschitzki, S. Chien, S. Weinbaum, A fiber matrix model for the growth of macromolecular leakage spots in the arterial intima, J. Biomech. Eng. 116 (1994) 430–445.

[10] Z.J. Huang, J.M. Tarbell, Numerical simulation of mass transfer in porous media of blood vessel walls, Am. J. Physiol. 273 (1997) H464–H477.

[11] S. Tada, J.M. Tarbell, Internal elastic lamina affects the distribution of macromolecules in the arterial wall: a computational study, Am. J. Physiol. 287 (2004) H905–H913.

[12] D.L. Fry, Mathematical models of arterial transmural transport, Am. J. Physiol. 248 (1985) H240–H263.

[13] D.L. Fry, Mass transport, atherogenesis and risk, Arteriosclerosis 7 (1987) 88–100.

[14] G. Karner, K. Perktold, H.P. Zehentner, Computational modeling of macromolecule transport in the arterial wall, Comput. Meth. Biomech. Biomed. Eng. 4 (2001) 491–504.

[15] O. Kedem, A. Katchalsky, Thermodynamic analysis of the permeability of biological membranes to non-electrolytes, Biochem. Biophys. Acta 27 (1958) 229–246.

[16] C.C. Michel, F.E. Curry, Microvascular permeability, Physiol. Rev. 79 (1999) 703–761.

[17] J.M. Tarbell, Mass transport in arteries and the localization atherosclerosis, Ann. Rev. Biomed. Eng. 5 (2003) 79–118.

[18] K. Vafai, C.L. Tien, Boundary and inertia effects on flow and heat transfer in porous media, Int. J. Heat Mass Transfer 24 (1981) 195–203.

[19] K. Vafai, C.L. Tien, Boundary and inertia effects on convective mass transfer in porous media, Int. J. Heat Mass Transfer 25 (1982) 1183–1190.

[20] B. Alazmi, K. Vafai, Analysis of fluid flow and heat transfer interfacial conditions between a porous medium and a fluid layer, Int. J. Heat Mass Transfer 44 (2001) 1735–1749.

[21] A.-R.A. Khaled, K. Vafai, The role of porous media in modeling flow and heat transfer in biological tissues, Int. J. Heat Mass Transfer 46 (2003) 4989–5003.

[22] K. Vafai, M. Sozen, Analysis of energy and momentum transport for fluid flow through a porous bed, ASME J. Heat Transfer 112 (1990) 690–699.

[23] G. Meyer, R. Merval, A. Tedgui, Effects of pressure-induced stretch and convection on low-density lipoprotein and albumin uptake in the rabbit aortic wall, Circ. Res. 79 (1996) 532–540.

[24] X. He, D.N. Ku, Pulsatile flow in the human left coronary artery bifurcation: average conditions, Trans. ASME 118 (1996) 74–82.

[25] I.V. Pivkin, P.D. Richardson, D.H. Laidlaw, G.E. Karniadakis, Combined effect of pulsatile flow and dynamic curvature on wall shear stress in a coronary artery bifurcation model, J. Biomech. 38 (2005) 1283–1290.

[26] F.E. Curry, Mechanics and thermodynamics of transcapillary exchange, in: E.M. Renkin (Ed.), Handbook of Physiology, vol. IV, Am. Physiol. Soc., Bethesda, Minnesota, 1984, Section 2, Part 1, Chapter 8.

[27] A.G. Ogston, The spaces in a uniform random suspension of fibers, Trans. Faraday Soc. 54 (1958) 1754–1757.

[28] A.G. Ogston, B.N. Preston, J.D. Wells, On the transport of compact particles through solutions of chain-polymer, Proc. Roy. Soc. Lond. A 333 (1973) 297–316.

[29] J.E. Schnitzer, Analysis of steric partition behavior of molecules in membranes using statistical physics, Application to gel chromatography and electrophoresis, Biophys. J. 54 (1988) 1065–1076.

[30] L.V. McIntire, R. Tran-Son Tray, Concentration of materials released from mural platelet aggregates: flow effects, in: W.J. Yang, J.L. Chun (Eds.), Biomedical Engineering, Hemisphere Publishing Corporation, New York, Washington, 1989, pp. 229–245.

[31] Y. Huang, S. Weinbaum, D. Rumschitzki, S. Chien, A fiber matrix model for the growth of macromolecular leakage spots in the arterial intima, Adv. Biol. Heat Mass Transfer HTD 231 (1992) 81–92.

[32] S. Lin, K. Jan, G. Schuessler, S. Weinbaum, S. Chien, Enhanced macromolecular permeability of aortic endothelial cells in association with mitosis, Arteriosclerosis 73 (1988) 223–232.

[33] S.H. Song, M.R. Roach, Quantitative changes in the size of fenestration of elastic laminas of sheep thoracic aorta studied with SEM, Blood Vessels 20 (1983) 145–153.

[34] C.B. Vargas, F.F. Vargas, J.G. Pribyl, P.L. Blackshear, Hydraulic conductivity of the endothelial and outer layers of the rabbit aorta, Am. J. Physiol. 236 (1979) H53–H60.

[35] G.A. Truskey, W.L. Roberts, R.A. Herrmann, R.A. Malinauskas, Measurement of endothelial permeability to ^{125}I-low density lipoproteins in rabbit arteries by use of en face preparations, Circ. Res. 71 (1992) 883–897.

[36] FIDAP Theory Manual, Fluent Inc., Lebanon, USA, 2003.

[37] K. Khanafer, K. Vafai, K. Kangarlu, Computational modeling of cerebral diffusion-application to stroke imaging, Magn. Reson. Imaging 21 (2003) 651–661.

[38] K. Khanafer, K. Vafai, K. Kangarlu, Water diffusion in biomedical systems as related to magnetic resonance imaging, Magn. Reson. Imaging 21 (2003) 17–31.

[39] A.-R.A. Khaled, K. Vafai, Analysis of oscillatory flow disturbances and thermal characteristics inside fluidic cells due to fluid leakage and wall slip conditions, J. Biomech. 37 (2004) 721–729.

[40] M.A. Katz, New formulation of water and macromolecular flux which corrects for non-ideality: theory and derivation, predictions, and experimental results, J. Theor. Biol. 112 (1985) 369–401.

[41] J.M. Tarbell, Bioengineering studies of the endothelial transport barrier, BMES Bull. 17 (1993) 35–39.

[42] A. Tedgui, M.J. Lever, Filtration through damaged and undamaged rabbit thoracic aorta, Am. J. Physiol. 247 (1984) H784–H791.

[43] G.A. Truskey, Low density lipoprotein transport and metabolism in the arterial wall, Ph.D. thesis, Massachusetts Institute of Technology, Cambridge, MA, 1985.
[44] E.D. Morris, G.M. Saidel, G.M. Chisolm, Optimal design of experiments to estimate LDL transport parameters in arterial wall, Am. J. Physiol. 261 (1991) H929–H949.
[45] C.K. Colton, S. Friedman, D.E. Wilson, R.A. Lees, Ultra filtration of lipoproteins through a synthetic membrane, J. Clin. Invest. 51 (1972) 2472–2481.
[46] K.H. Keller, The influence of shear dependent diffusion in blood on atherogenesis and thrombogenesis, in: R.M. Nerem (Ed.), Fluid Dynamics Aspects of Arterial Disease, Ohio State University, Ohio, 1974, pp. 43–45.
[47] J.M. Tarbell, M.J. Lever, C.G. Caro, The effects of varying albumin concentration on the hydraulic conductivity of the rabbit common carotid artery, Microvasc. Res. 35 (1988) 204–220.
[48] X. Deng, Y. Marois, T. How, Y. Merhi, M. King, R. Guidoin, Luminal surface concentration of lipoprotein (LDL) and its effect on the wall uptake of cholesterol by canine carotid arteries, J. Vasc. Surg. 21 (1995) 135–145.
[49] V.S. Warty, W.J. Calvo, S.A. Berceli, S.M. Pham, S.J. Durham, S.K. Tanksale, E.C. Klein, I.M. Herman, H.S. Borovetz, Hemodynamics alter arterial low-density lipoprotein metabolism, J. Vasc. Surg. 10 (1989) 392–399.
[50] C.G. Caro, J.M. Fitz-Gerald, R.C. Schroter, Atheroma and arterial wall shear. Observation, correlation and proposal of a shear dependent mass transfer mechanism for atherogenesis, Proc. Roy. Soc. Lond. B Biol. Sci. 177 (1971) 109–159.
[51] D.N. Ku, D.P. Giddens, C.K. Zarins, S. Glagov, Pulsatile flow and atherosclerosis in the human carotid bifurcation. Positive correlation between plaque location and low oscillating shear stress, Arteriosclerosis 5 (1985) 293–302.
[52] M.H. Friedman, C.B. Bargeron, O.J. Deters, G.M. Huchins, F.F. Mark, Correlation between wall shear and intimal thickness at a coronary artery branch, Atherosclerosis 68 (1987) 27–33.
[53] S.A. Berger, L.-D. Jou, Flows in stenotic vessels, Ann. Rev. Fluid Mech. 32 (2000) 347–382.
[54] D.N. Ku, Blood flow in arteries, Ann. Rev. Fluid Mech. 29 (1997) 399–434.